Heliyon 10 (2024) e36024

Contents lists available at ScienceDirect

Heliyon

journal homepage: www.cell.com/heliyon

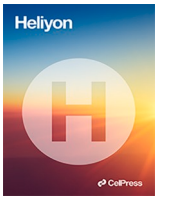

Research article

Hyperuricemia drives intestinal barrier dysfunction by regulating gut microbiota

Xiaomin Yang [a], Dan Liu [c], Xiangzhong Zhao [b], Yafei Han [b], Xiao Zhang [b], Quan Zhou [b], Qiulan Lv [b,*]

[a] *Laboratory Medicine, the Affiliated Hospital of Qingdao University, Qingdao, 266003, PR China*
[b] *Medical Research Center, the Affiliated Hospital of Qingdao University, Qingdao, 266003, PR China*
[c] *Laboratory Medicine, Qingdao Fuwai Cardiovascular Hospital, PR China*

ARTICLE INFO

Keywords:
hyperuricemia
Gut microbiota
Intestinal permeability
Metabolic disorder

ABSTRACT

Background: Hyperuricemia elevates gut permeability; however, the risk of its influence on the compromised intestinal barrier is poorly understood.
Aims: This study was carried out, aiming to elucidate the orchestrators and disruptors of intestinal barrier in hyperuricemia.
Methods: A mouse model of hyperuricemia was induced by administering adenine and oteracil potassium to mice. Allopurinol was used to decrease uric acid level, and antibiotics were administered to mice to deplete gut microbiota. Intestinal permeability was assessed using FITC-labeled dextran. Changes in gut microbial community were analyzed through 16S rRNA sequencing. IL-1β and TNF-α levels were quantified using ELISA. The expression of tight junction protein genes, *TLR4*, *p65* and *IL-1β*, was determined with Q-PCR and Western blotting.
Results: Allopurinol treatment effectively reduced intestinal permeability and serum TNF-α levels. Antibiotic treatment alleviated but not abolished intestinal permeability. Uric acid alone was insufficient to increase Coca2 monolayer permeability. Allopurinol treatment altered microbial composition and suppressed opportunistic infections. Re-establishing hyperuricemia in a germ-free mouse model protected mice from intestinal injury. Allopurinol and antibiotic treatments reduced *TLR4* and *IL-1β* expressions, increased *occludin* and *claudin-1* expressions but suppressed NF-κB p65 signaling. However, removing gut microbiota aggravated lipid metabolic dysfunction.
Conclusion: Gut microbiota is a direct and specific cause for intestinal barrier dysfunction.

1. Introduction

Hyperuricemia has been emerged as a burgeoning epidemic metabolic disease and increases the risk of obesity, diabetes, hypertension and cardiovascular diseases [1–3]. Most treatments focus on kidney from the perspective of lowing serum uric acid level; however, effective treatments remain elusive. Recently, studies have shown that intestinal barrier dysfunction is associated with metabolic syndrome [4], which is attracting increasing attention.

The intestinal barrier comprises various structural and functional components, which form a coordinated and dynamic network responding the dynamic microenvironment [5,6]. Increased intestinal barrier allows the entry of microbial antigens, toxins and

* Corresponding author. No.1677, Wutai Mountain Road, Affiliated Hospital of Qingdao University, Qingdao, 266003, PR China.
E-mail address: lvqiulan@qdu.edu.cn (Q. Lv).

https://doi.org/10.1016/j.heliyon.2024.e36024
Received 3 April 2024; Received in revised form 6 August 2024; Accepted 8 August 2024
Available online 9 August 2024
2405-8440/© 2024 Published by Elsevier Ltd. This is an open access article under the CC BY-NC-ND license (http://creativecommons.org/licenses/by-nc-nd/4.0/).

inflammatory mediators into the systemic circulation, which, in turn, initiates a vicious cycle of systemic low-grade inflammation. Increasingly, researchers have been showing that the dysfunction of the intestinal barrier features metabolic syndrome [7,8]. In mouse models of obesity and diabetes, previous studies have shown that hyperglycemia drives intestinal barrier permeability through GLUT2-dependent transcriptional reprogramming, resulting in enhanced systemic infection and inflammatory responses [4]. Alcohol-induced tissue damage and organ dysfunction are also associated with increased intestinal permeability [9]. Recently, evidences has highlighted hyperuricemia as a distinctive feature of compromised intestinal barriers, which is accompanied by an increased systemic tumor necrosis factor (TNF-α) and lipopolysaccharide (LPS) levels [10–12]. More than one third of uric acid is excreted through intestine, and dysfunction of intestine increases the risk of hyperuricemia [13]. Our previous studies demonstrated a positive correlation between elevated uric acid and increased intestinal permeability [10], which evidenced the important role of intestinal barrier. Thus, elucidating the orchestrators and disruptors of the intestinal barrier in hyperuricemia is momentous for the treatment of hyperuricemia and its complications. However, the mechanism underlining the influence of hyperuricemia on the intestinal barrier is poorly understood.

Intrinsic and extrinsic stimuli including abnormal acidity, alcohol and inflammation can instigate compromised intestinal barrier [14]. *In vitro* studies have shown that elevated uric acid can promote oxidative stress and inflammation, and further disrupte tight junctions [15,16]. Recently, microbiota has been emerged as a key regulator of intestinal barrier function by activating toll-like receptors (TLRs) [17,18]. In mouse models of obesity and diabetes, studies have shown that it is hyperglycemia rather than microbial change plays a critical role in glucose-mediated barrier dysfunction. Emerging evidences have shown that hyperuricemia is characterized by gut microbiota dysbiosis [19]. However, in mouse mode of hyperuricemia, whether the increased intestinal permeability is

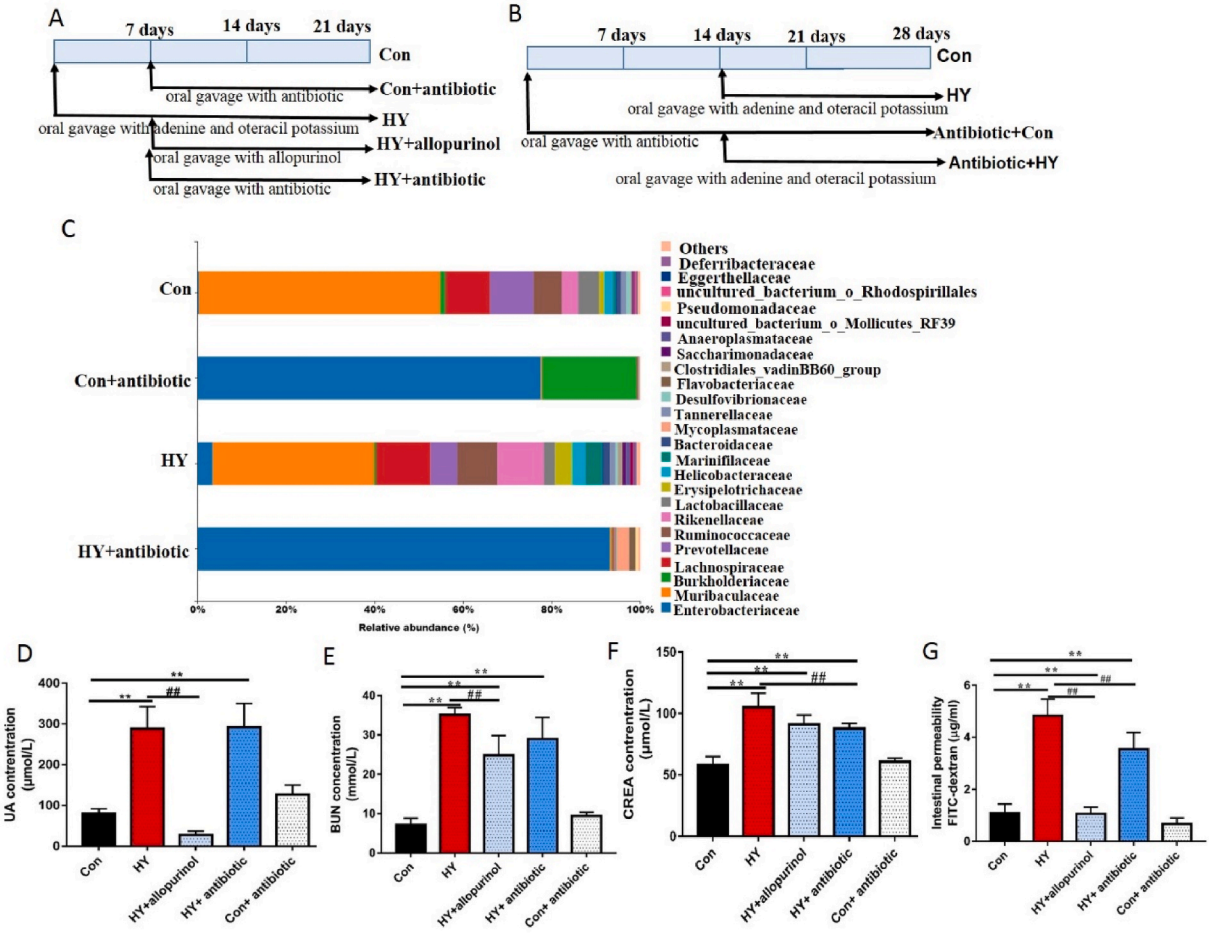

Fig. 1. Both hyperuricemia and gut microbiota were associated with intestinal barrier dysfunction. (A–B) The experimental protocol. (C) The relative abundance of the total gut community at family level after oral administration of antibiotic for two weeks on mouse model of hyperuricemia, as determined by 16S rRNA gene sequencing of stool. n = 5 mice per group. (D–F) Serum levels of UA (D), BUN (E) and CREA detected using an automatic biochemical analyzer after treatment with allopurinol or antibiotic for two weeks. n = 6 mice per group. (G) FITC-dextran recovered from the serum after oral gavage allopurinol and antibiotic for two weeks. n = 6 mice per group. NC, control group; HY, hyperuricemia mice. Bars and error bars represent the Means ± SEM, respectively. $^{**}p < 0.01$ verse Con or $^{\#\#}p < 0.01$ verse HY using one-way ANOVA followed by Tukey's multiple comparison post-test.

result from elevated uric acid or alternated microbial composition remains unknown. Although researchers are actively investigating these relationships to gain deeper insights into the underlying mechanism, a definitive cause-and-effect relationship has not yet been established.

To elucidate the mechanism of compromised intestinal barrier in hyperuricemia, we performed systemic studies *in vitro* and *in vivo*. We comprehensively documented the effect of uric acid and gut microbiota on intestinal barrier, and deciphered the mechanisms including lowering uric acid, removing gut microbiota and re-establishing hyperuricemia in a germ-free mouse model. Our findings provided targeted interventions for ameliorating hyperuricemia and the related complications from a novel perspective.

2. Materials and method

2.1. Mouse models

These experiments were conducted according to established animal welfare guidelines. The experiments were approved by the Affiliated Hospital of Qingdao University of Animal Care Committee (AHQU-mal2018079), and the study complied with all regulations. C57BL/6J mice, six weeks old, male (Beijing Vital River Laboratory Animal Technology Co., Ltd., Beijing, China), were acclimatized for two weeks in a 12 h light – 12 h dark illuminance rhythm before experiments. Mice were randomly assigned to experimental groups, 6 mice each. Hyperuricemia (HY) was established through daily intragastric administration of adenine (50 mg/kg) and oteracil potassium (125 mg/kg) (diluted in 0.5 % of carboxymethyl cellulose sodium) for 21 days [20]. The control group (Con) received intragastric 0.5 % of carboxymethyl cellulose sodium alone. On day 7, HY groups were treated with allopurinol (50 mg/kg) or antibiotic (5 mg of vancomycin, 100 mg of metronidazole, 100 mg of neomycin, and 100 mg of ampicillin) or PBS *via* gavage for the remaining 14 days. Con groups received PBS or antibiotic at the same intervals (Fig. 1A). All procedures were performed in compliance with relevant laws and institutional guidelines and that the appropriate institutional committee have approved them.

For antibiotic experiment, mice received oral antibiotics for 14 days, followed by oral gavage with adenine and oteracil potassium to established hyperuricemia model, or 0.5 % of carboxymethyl cellulose sodium as control. Oral gavage of antibiotics continued throughout the experiments (Fig. 1B). Blood samples were collected by retro-orbital bleeding after an overnight fast at various time points. Biochemical indicators, including serum uric acid, triglyceride (TC), total cholesterol (TG), and high- and low-density lipoprotein cholesterols (HDL and LDL), creatinine (CREA) and urea nitrogen (BUN) were determined using an automatic biochemical analyzer (Toshiba, Tokyo, Japan). At the end of experiments, fecal, blood and colon tissue samples were collected and frozen in liquid nitrogen immediately.

2.2. Microbiome sequencing analysis

The V3–V4 regions of 16S rRNA gene were amplified with specific primers, 319f 5′-ACT CCT ACG GGA GGC AGC AG-3′ and 806r 5′-GGA CTA CHV GGG TWT CTA AT-3′, for the analysis of microbiomes. The amplicons were purified using AxyPrep DNA GelExtraction Kit (Axygen Biosciences, Union City, CA, USA) and quantificated with QuantiFluor-ST (Promega, Madison, WI, USA). The qualified amplicons were paired-end sequenced on an Illumina Novaseq 6000 according to the standard protocol by Beijing Biomarker Technology. Raw reads were quality filtered using Trimmomatic v0.33 and primer removed using cutadapt 1.9.1 to clean ones. After merging paired ends, error correction and chimera detection, OTUs with 97 % similarity cutoff were clustered using UPARSE v10. The taxonomy each OTU representative sequence was analyzed with Ribosomal Database Project (RDP) Classifier v.2.2. Alpha diversity index was estimated using QIIME 2. Principal Coordinate Analysis (PCoA) based on weighted and Bray-Curtis dissimilarity was used to identify microbial community structure. Linear discriminant analysis effect size (LEfSe) was performed to identify differentially enriched bacterial taxa with LDA logarithmic score above 3.0. A Wilcoxon rank-sum test (FDR <0.05) was performed to identify the differential bacterial taxa between two groups. The sequencing data have been deposited in NCBI Sequence Read Archive (PRJNA1059487).

2.3. Serum levels of TNF-α and IL-1β measurements

Blood samples were collected at a specific time period, and centrifuged at 3000 rpm for 10 min to isolate serum. Serum concentrations of TNF-α and IL-1β were measured in duplicate using mice TNF-α ELISA Kit and mice IL-1β ELISA Kit (Mibio, China) ($n = 6$) following the instructions. Standard samples were used to create the concentration standard curve. Absorbance at 405 nm was read on a microplate reader. The TNF-α and IL-1β antibody concentrations were calculated based on the standard curve.

2.4. Blood and urine measurements

Blood samples of all groups were collected from the suborbital vein at a specific time period. The sample was then centrifuged at 3000 rpm for 10 min to acquire serum. Serum concentrations of TG, TC, HDL, LDL, creatinine and urea nitrogen were measured using a 7020 automatic biochemistry analyzer (Hitachi Ltd., Tokyo, Japan).

2.5. Mouse intestinal permeability assay

Mice were administered 40 mg 4-kDa FITC-labeled dextran (FD4; Sigma–Aldrich) per 100 g body weight after a 4-h water and food

deprivation. Four hours later, blood was obtained through retro-orbital bleeding and subsequently centrifuged at 2000 rpm for 10 min. Serum samples were assayed for FITC fluorescence at 485 nm excitation and 530 nm emission using a TECAN Infinite M200 plate reader. Concentrations of FITC-dextran were quantified based on a standard curve.

2.6. Cell culture and in vitro permeability measurement

Caco-2 cells (human, ATCC, HTB-37) were seeded at a density of 6×10^5 cells/mL on 12-well Polycarbonate Membrane Transwell Inserts with the pore size of 0.4 μm (Corning Life Sciences), and cultured for 10–14 days. Subsequently, Caco-2 cells were exposed to 6 mg/dL of soluble uric acid for 24 and 48h, respectively. After the removal of the culture medium, 250 μg/mL FITC-labeled dextran (4 kDa; Sigma-Aldrich) was added to the apical compartment. The basolateral compartment was filled with 1 mL of the same medium without FITC dextran and the transwells were cultured at 37 °C for 2h. Concentration of FITC–dextran in the basolateral compartment was measured in duplicate using a TECAN Infinite M200 plate reader with excitation at 485 nm and emission at 530 nm. Values were expressed as a percentage of the average control value.

2.7. RNA isolation and gene expression analyses

Total RNAs were extracted from the colon using TRIzol reagent (Life Technologies, United States) following the manufacturer's instructions. The cDNA was synthesized using a PrimeScript RT reagent kit (Takara, Tokyo, Japan) following manufacturer's instructions. Real-time PCR was performed in triplicate with an SYBR Premix Ex Taq Kit (Takara, Kyoto, Japan). The specific primers for *Occludin* (Gene ID 18260) were 5′- TTG AAA GTC CAC CTC CTT ACA GA T CTC AAA GAC-3′ (, orward) and 5′- CCG GAT AAA AAG AGT ACG CTG G-3′ (reverse). The primers specific for *ZO-1* (Gene ID 21872) were 5′-ACT CCC ACT TCC CCA AAA AC-3′ (forward) and 5′- CCA CAG CTG AAG GAC TCA CA-3′ (reverse). The specific primer of *Claudin-1* (Gene ID 12737) were 5′- AGA TAC AGT GCA AAG TCT TCG A-3′ (forward) and 5′- CAG GAT GCC AAT TAC CAT CAA G-3′ (reverse). The specific primers for *GAPDH* (Gene ID 14433) were 5′- ATC TCC ACT TTG CCA CTG C-3′ (forward) and 5′- ACA TTG GGG GTA GGA ACA CGG A-3′ (reverse). All primers were verified for the production of a single specific PCR product with a melting curve program. The fold increase of transcript abundance was calculated with the 2^(−ΔΔCT) method and normalized to that of *GAPDH* as an internal control.

2.8. Western blot analysis

Total proteins from colon tissues were extracted using homogenised lysis buffer containing 1 % PMSF. After smashing using high throughput tissue grinder, supernatant containing total proteins was collected and resolved through by SDS-PAGE and transferred onto the polyvinylidene fluoride membranes (Millipore, MA, United States). The membranes were blocked with 5 % skimmed milk for 2 h at room temperature and then incubated with the following primary antibodies, mouse anti-TLR4 (Cat# sc-293072, 1:500, Santa Cruz Biotechnology, United States), rabbit anti-IL-1b (Cat# ab9722, 1:1000, Abcam), mouse anti-occludin (Cat# 33–1500, 1:1500, Thermo Fisher Scientific, United States) and rabbit anti-claudin-1 (Cat# NBP1-77036, 1:1000, Novus), rabbit anti-ZO-1 (Cat# AF5154, 1:1000, Affinity Biosciences, United States), rabbit anti–NF–κB p65(Cat# cst 8242, 1:1000, Cell Signaling Technology, United States) and rabbit anti-Phospho–NF–κB p65(Cat# cst 3033, 1:1000, Cell Signaling Technology, United States) at 4_C overnight, and then with the secondary antibodies at room temperature (RT) for 1 h. The protein signals were detected on an imaging system using a chemiluminescence kit (Millipore, MA, United States) and analyzed using Image-Pro Plus software (Bio-Rad, United States). *ß-actin* and *GAPDH* was used as the internal loading control.

2.9. Statistical analyses

Bars and error bars represent the mean and standard error of the mean (SEM). Normal distribution was tested using Shapiro-Wilk test. The comparisons of more than three groups were analyzed by ANOVA, which was followed by with Tukey tests using SPSS 17.0 under the condition of the normal distribution. The differential bacteria between group was tested by LEfSe. P-values <0.05 indicated statistically significant differences.

3. Results

3.1. Hyperuricemia is associated with but not required for intestinal barrier dysfunction

To investigate the drivers of intestinal barrier dysfunction in hyperuricemia, we explored the roles of uric acid and gut microbiota in regulating barrier integrity. As showed in Fig. 1C, antibiotic treatment depleted almost all of commensals. Compared with HY group, allopurinol treatment significantly reduced uric acid ($P = 0.00$) and BUN ($P = 0.00$) levels. Compared with HY group, antibiotic treatment had no effect on uric acid (P = 0.99) and BUN ($P = 0.08$) levels, but significantly decreased CREA level ($P = 0.00$) (Fig. 1D–F). There was no difference in uric acid ($P = 0.33$), BUN ($P = 0.84$) and CREA ($P = 0.97$) levels between Con and Con with antibiotic addition groups.

We proceeded to investigate the impact of uric acid and gut microbiota on intestinal barrier. Compared with Con group, intestinal permeability robustly rised in HY group ($P = 0.00$) but significantly reduced if treated with allopurinol ($P = 0.00$). Surprisingly, compared with HY group, antibiotic treatment significantly ameliorated gut permeability ($P = 0.00$). However, gut permeability in HY

with antibiotics treatment group remained higher than that in Con group ($P = 0.00$) (Fig. 1 G). No significant difference was observed between the Con and Con with antibiotics addition groups ($P = 0.60$). Collectively, these results suggested that hyperuricemia *per se* may not provide a sufficient explanation to barrier dysfunction.

3.2. Allopurinol alleviates systemic inflammation by reducing uric acid

We further assessed whether the changes of uric acid and gut microbiota have effect on systemic inflammation. As showed, there was no difference of circulating IL-1β among all groups (Fig. 2A). HY mice exhibited elevated systemic TNF-α levels ($P = 0.00$). In contrast, TNF-α level was reduced to that of controls after treatment with allopurinol ($P = 0.00$, HY + allopurinol *vs* HY; $P = 0.99$ HY + allopurinol *vs* Con). However, compared with HY group, antibiotic treatment slightly increased systemic TNF-α level ($P = 0.56$) (Fig. 2B). Compared with Con group, LDL ($P = 0.00$), HDL ($P = 0.00$), TC ($P = 0.01$) and TBA ($P = 0.00$) levels were significantly elevated in HY group (Fig. 2D–F). However, allopurinol treatment markedly reduced LDL level ($P = 0.00$) and slightly decreased HDL ($P = 0.28$) and TC ($P = 0.92$) levels compared with HY group. Antibiotics treatment showed a less pronounced effect on LDL, HDL, TC and TBA levels when compared with HY group (Fig. 2C–E). Notably, compared with Con group, HDL ($P = 0.00$), TC ($P = 0.00$) and TBA ($P = 0.95$) levels were also elevated in Con + antibiotics group. The level of TG did not show significant difference among all groups

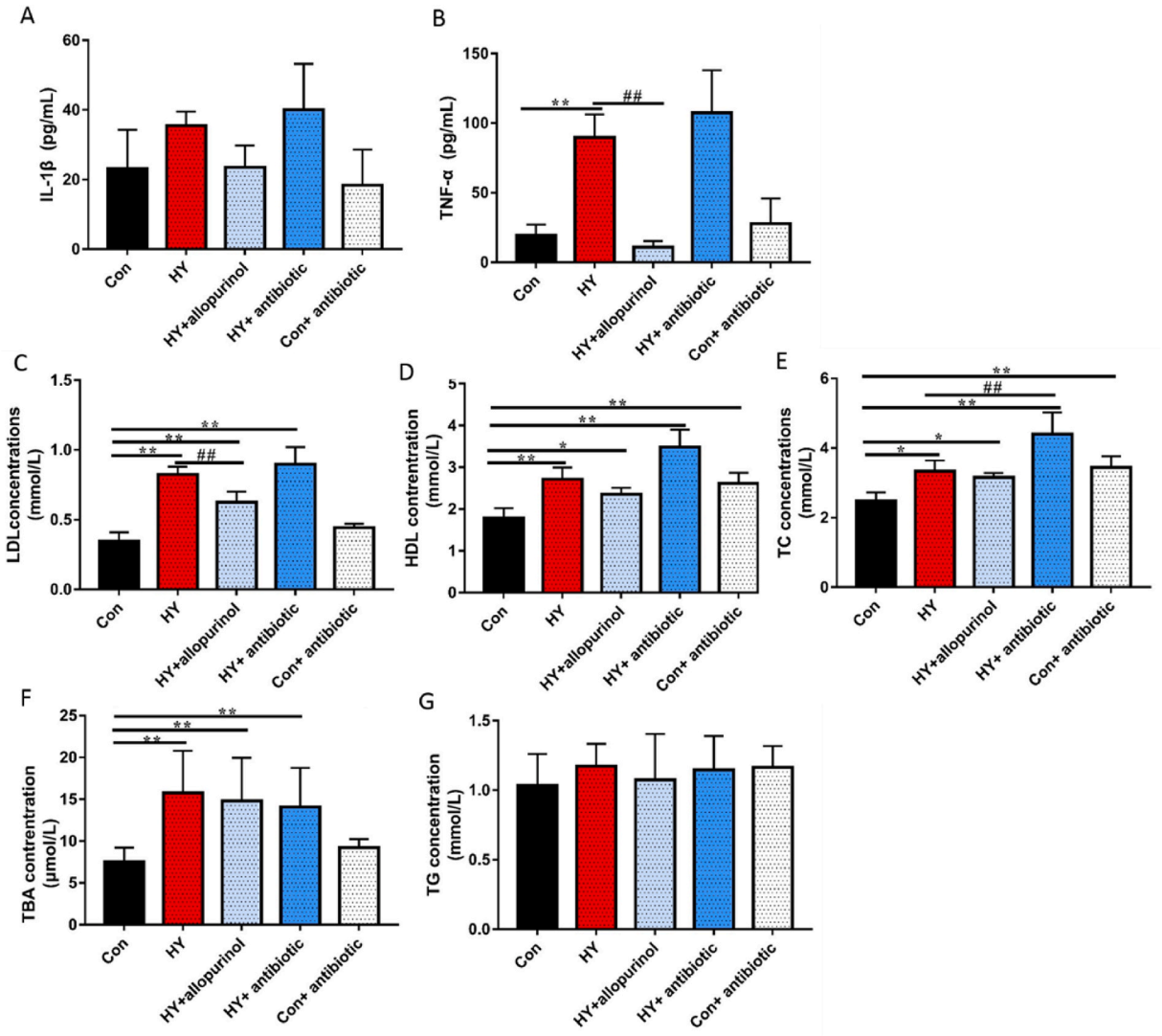

Fig. 2. Lowering uric acid level alleviates systemic inflammation and lipid metabolism. (A–B) Serum levels of IL-1β (A) and TNF-α (B) were detected using ELISA after treatment with allopurinol or antibiotic. (C–G) Serum levels of LDL (C), HDL (D), TC (E), TBA (F), and TG (G) were detected using an automatic biochemical analyzer after treatment with allopurinol or antibiotic. n = 6 mice per group. NC, control group; HY, hyperuricemia mice. Bars and error bars represent the Means ± SEM, respectively. *p < 0.05, **p < 0.01 verse Con, ##p < 0.01 verse HY using one-way ANOVA followed by Tukey's multiple comparison post-test.

(Fig. 2 G).

3.3. Allopurinol upregulates junctional protein expression by suppresing TLR4/P65

To elucidate the mechanism underlying the ameliorative effects of allopurinol on hyperuricemia-induced barrier damage, a comprehensive investigation was undertaken which was focused on TLR4 and proinflammatory factors. Compared with HY group,

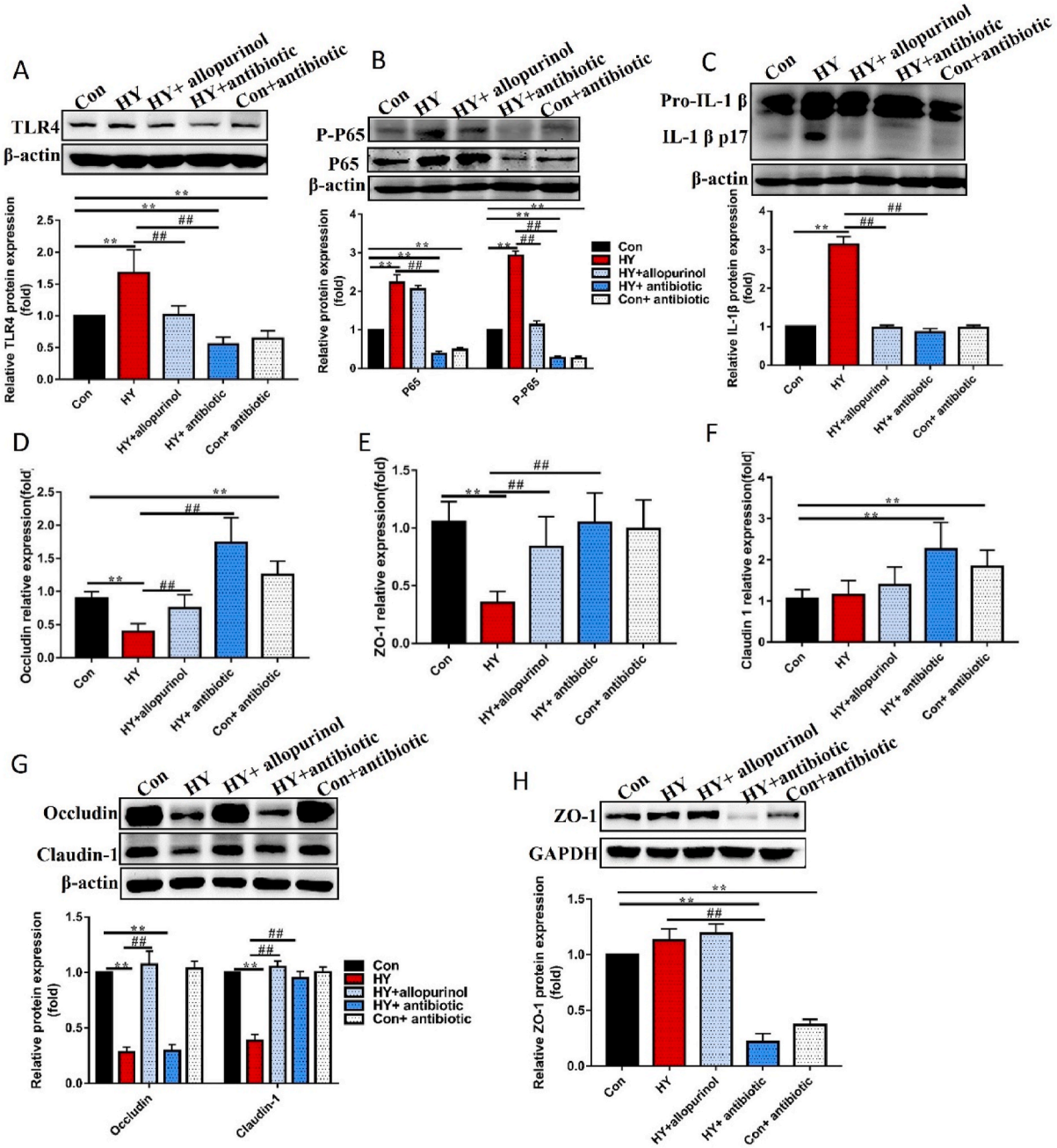

Fig. 3. Allopurinol upregulates junctional protein expression by suppressing TLR4/P65. (A–C) Representative immunoblotting of TLR4 (A), P65 (B) and IL-1β (C) from isolated colon after treatment with allopurinol or antibiotic. (D–F) Relative expression levels of Occludin (D), ZO-1 (E) and Claudin1 (F) genes were determined by Q-PCR from isolated colon after treatment with allopurinol or antibiotic. n = 6 mice per group. (G and H) Representative immunoblotting of Occludin, Claudin1 (G) and IL-1β (H) from isolated colon after treatment with allopurinol or antibiotic. NC, control group; HY, hyperuricemia mice. Bars and error bars represent the Means ± SEM. *p < 0.05, **p < 0.01 verse Con, $^{\#\#}$p < 0.01 verse HY using one-way ANOVA followed by Tukey's multiple comparison post-test.

both allopurinol and antibiotic treatment significantly reduced TLR4 expression suppressed NF-κB p65 activation and inhibited IL-1β release (Fig. 3A–C). At transcript levels, compared with Con group, the HY group exhibited lower levels of occludin ($P = 0.00$) and ZO-1 ($P = 0.00$), which were effectively reversed by both allopurinol and antibiotic treatments (Fig. 3D and E). Compared with Con, Claudin-1 transcription was significant upregulated in HY + antibiotic ($P = 0.00$) and Con + antibiotic groups($P = 0.00$) (Fig. 3 F). At protein level, compared to the HY group, allopurinol treatment significantly upregulated occludin ($P = 0.00$) and Claudin-1 ($P = 0.00$) expression. Similarly, antibiotic treatment upregulated Claudin-1($P = 0.00$), but not affected occludin expression ($P = 0.98$) when compared to HY group (Fig. 3G). No difference of ZO-1 protein was observed between Con and HY groups ($P = 0.00$). However, compared with Con group, ZO-1protein level was reduced in Con + antibiotic group ($P = 0.00$) (Fig. 3H). These data underscored that lowering uric acid can rescue gut barrier by alleviating inflammation and upregulating junctional protein expression.

3.4. Allopurinol rescues intestinal barrier by changing gut microbiota

We subsequently investigated whether allopurinol may restore the barrier function or not with the mediation of gut microbiota. Compared with WT mice, HY mice exhibited significantly elevated Ace and Shannon indices. Allopurinol treatment restored the Shannon index but not the Ace index comapre with HY grop (Fig. 4A and B). Principal coordinate analysis (PCoA) based on weighted unifrac distance demonstrated a clear separation among Con, HY, and HY + allopurinol groups. Notably, the gut microbial community structure of the HY + allopurinol group exhibited a trajectory distinct from that of the HY group (Fig. 4C).

We further analyzed the differential bacteria by LEfSe (LDA> 3.0). Compared with Con group, the richness of 44 bacteria was elevated and that of 21 bacteria was depleted in HY group (Fig. 4 D). Following allopurinol treatment, compared with HY group, the abundance of 53 bacteria altered (differential bacteria), which included 33 elevated and 20 reduced (Fig. 4 E). Remarkably, allopurinol treatment reversed the increased abundance of families such as Eggerthellaceae, Erysipelotrichaceae, Marinifilaceae, Saccharimonadaceae, Streptococcaceae and uncultured_bacterium_o_Mollicutes_RF39, and simultaneously reversed the decreased abundance of Tannerellaceae observed in HY group (Fig. 4 F). Similarly, the abundance of genera ASF356, Candidatus_Saccharimonas, Lactococcus, Rikenellaceae_RC9_gut_group, Staphylococcus, Streptococcus and Turicibacter was restored to that of control by allopurinol treatment (Fig. 4 G).

3.5. Gut microbiota is the major driver for intestinal barrier dysfunction

To test whether the elevated uric acid level is the major driver for barrier dysfunction, we performed *in vitro* experiments. We found that uric acid alone did not increase Caco-2 monolayers permeability (Fig. 5 A).

To verify the specificity of gut microbiota as a driver of intestinal barrier, we administered antibiotics to mice for a period of two weeks prior to inducing hyperuricemia. Antibiotics effectively depleted a significant portion of the gut microbiota (Fig. 5 B). Compared with Con group, uric acid level in both HY and antibiotic + HY group was significant elevated in third and fourth week. However, compared with HY group, uric acid level in the antibiotic + HY group was significant lower than that in HY group (Fig. 5C). Intriguingly, compared with Con group, the HY group exhibited a corresponding increase in gut permeability in third and fourth week. However, intestinal permeability was reduced in antibiotic + HY group in third and fourth week (Fig. 5 D). Collectively, these results suggested that it is the gut microbiota, rather than uric acid, that served as a direct and specifically contributes to intestinal barrier dysfunction.

3.6. Gut microbiota is indispensable to lipid metabolic

We further determined whether the resuced intstinal barrier by antibiotics can alleviate systemic inflammation and lipid metabolic. No significant change was found in TNF-α ($P = 0.78$) and IL-1β ($P = 0.97$) levels between HY and antibiaotic + HY group (Fig. 6A–B). Furthermore, compared with Con group, levels of HDL, TC, LDL and TBA in both Antibiotic + HY and Antibiotic + Con groups increased significantly (Fig. 6C–F). No significant change was found in TG level among different groups (Fig. 6G). Interestingly, compared to the HY group, there was a significant reduction in CREA and BUN levels in Antibiotic + HY group (Fig. 6H–I).

3.7. Gut microbiota regulation of hyperuricemia intestinal barrier via the TLR4/P65 signal pathway

We further deciphered how microbiota affects gut barrier under hyperuricemia condition. Compared with Con group, TLR4 ($P = 0.00$), P65 ($P = 0.00$) and P–P65 ($P = 0.00$) expressions were elevated in HY group while their expressions were attenuated in Antibiotic + HY group ($P = 0.00$) (Fig. 7 A). Furthermore, compared with Con group, IL-1β was increased in HY group ($P = 0.00$), and reduced in antibiotic + HY group compared with HY group ($P = 0.00$) (Fig. 7 B). Moreover, compared with HY group, antibiotic pre-treatment significantly upregulated the expression of *Occludin* gene ($P = 0.00$) and the synthesis of Occludin ($P = 0.00$). Compared with HY group, claudin-1 was influenced in antibiotic + HY group only at the protein level ($P = 0.00$) (Fig. 7C–E-F). Notably, antibiotic pre-treatment upregulated ZO-1 at the mRNA level (P = 0.00), but significantly reduced ZO-1 protein levels (P = 0.00) (Fig. 7D–G). These results indicated that depletion of gut microbiota in hyperuricemia enhances the expression of tight junction protein by inhibiting the TLR4/P65 signaling pathway.

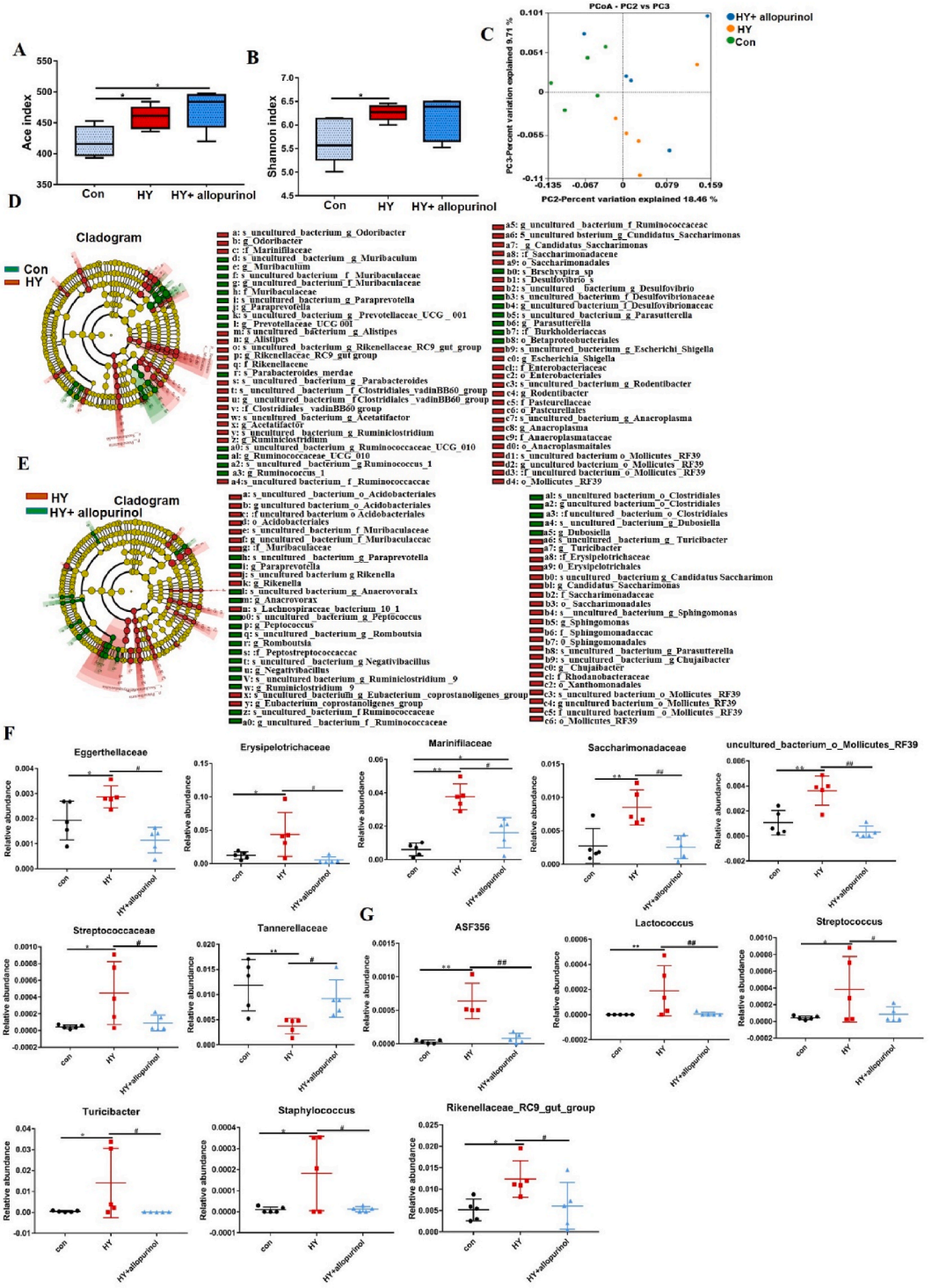

(caption on next page)

Fig. 4. Allopurinol treatment reverses gut microbiota. (A and B) α diversity presented as ACE (A) and Shannon (B) index after treatment with allopurinol for two weeks. (C) Principal coordinates analysis (PCoA) of gut microbiota composition based on weighted unifrac after treatment with allopurinol for two weeks. PCoA2 and PCoA3 represent the top two principal coordinates that capture most of the diversity. n = 5 mice per group. The cladogram was analyzed using A linear discriminant analysis effect size (LEfSe) to represent diferentially abundant taxa from Con (Green) and HY (red) (D), or HY (red) and HY + allopurinol (Green) (E). Only taxa with a statistically significant LDA score >3.0 were showed. Each node denotes a taxonomic unit within the bacterial hierarchy and nodes of different colors represent the crucial microbiome. Diameter of the small circle is proportional to the relative abundance. n = 5 mice per group. (F and G) The taxa at family (F) and genus (G) that were rescued to normal levels. n = 5 mice per group. NC, control group; HY, hyperuricemia mice. Bars and error bars represent the Means ± SEM. *p < 0.05, **p < 0.01 verse Con, $^{\#\#}$p < 0.01 verse HY using one-way ANOVA followed by Tukey's multiple comparison post-test. (For interpretation of the references to color in this figure legend, the reader is referred to the Web version of this article.)

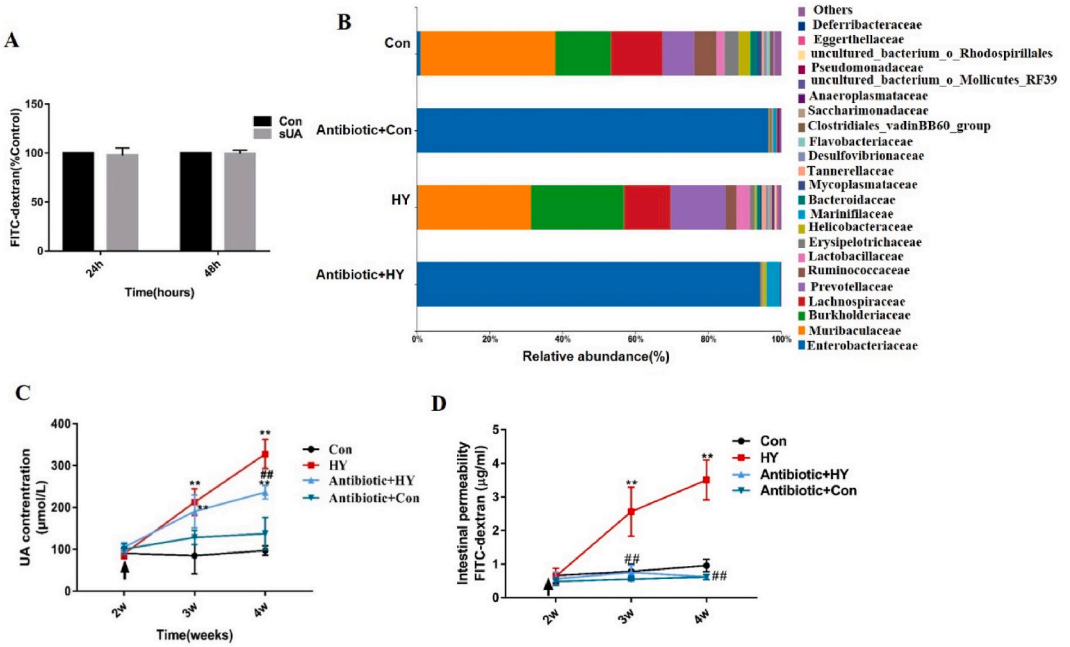

Fig. 5. Gut microbiota is the major driver for intestinal barrier dysfunction. (A) Paracellular permeability was determined by the flux of FITC–dextran through the Caco-2 monolayers. (B) The relative abundance of the total gut community at family level after administration of adenine and potassium oxalate for two weeks on mouse model of antibiotic induced germfree mice, as determined by 16S rRNA gene sequencing of stool. n = 5 mice per group. (C)Serum levels of UA at different time points after administration of adenine and potassium oxalate. Arrows present the time starting administration of adenine and potassium oxalate. n = 6 mice per group. (D) FITC-dextran recovered from the serum at different time points after oral gavage adenine and potassium oxalate. n = 6 mice per group. NC, control group; HY, hyperuricemia mice. Bars and error bars represent the Means ± SEM. *p < 0.05, **p < 0.01 verse Con, $^{\#\#}$p < 0.01 verse HY using repetitive measurement deviation analysis.

4. Discussion

Intestinal barrier dysfunction is the feature of metabolic diseases. Increased intestinal permeability leads to translocation of microbial components into systemic circulation, resulting in systemic inflammation and contributing to disease progression [21]. Emerging evidence has highlighted the association of hyperuricemia with elevated gut permeability. However, the specific mechanisms and actors played in this process remained elusive. In this study, we identified gut microbiota as a key orchestrator of compromised intestinal barrier in hyperuricemia. Lowering uric acid with allopurinol effectively rescued intestinal barrier and systemic inflammation. However, depletion of gut microbiota alleviated intestinal barrier under high uric acid level conditions, ruling out that uric acid *per se* directly drives the barrier dysfunction. Re-establishing hyperuricemia in a germ-free mouse model restored intestinal barrier despite of high uric acid level. These results supported the role of gut microbiota as a direct and specific driver for intestinal barrier dysfunction. However, antibiotic treatment aggravated lipid metabolic dysfunction, highlighting the indispensable role of gut microbiota in lipid metabolism.

Increasing evidences have strenthened the concept that intestinal barrier dysfunction causes metabolic dysfunction. The compromised intestinal barrier allows the translocation of pathogen-associated molecular patterns (PAMPs) into the bloodstream, and then activates innate immune response [22,23]. Previous researches showed that hyperuricemia is associated with compromised inteastinal barrier [12,20]; however, the mechanism has not been deciphored yet. Here, we revealed that uric acid is highly correlated with but not required for intestinal barrier dysfunction. Uric acid has been implicated as a danger signal [24]; however, such claim was primarily based on high uric acid level. Recently, microbiota has emerged as a key regulator of intestinal barrier function [25]. Studies

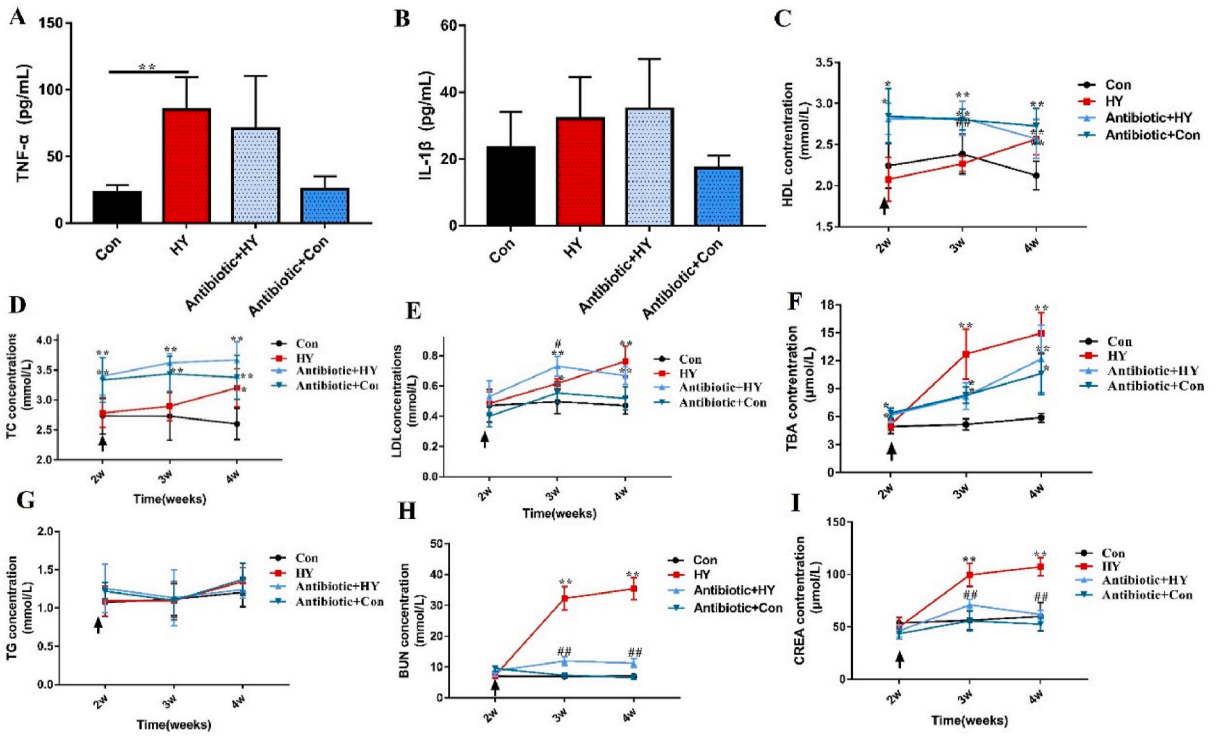

Fig. 6. Depletion of gut microbiota aggerates lipid metabolic dysfunction. (A and B) Serum levels of IL-1β (A) and TNF-α (B) were detected using ELISA after administration of adenine and potassium oxalate for two weeks on mouse model of antibiotic induced germfree mice. (C–I) Serum levels of HDL (C), TC (D), LDL (E), TBA (F), TG (G), BUN (H), and CREA(I) were detected using an automatic biochemical analyzer after after administration of adenine and potassium oxalate for two weeks on mouse model of antibiotic induced germfree mice. n = 6 mice per group. NC, control group; HY, hyperuricemia mice. Bars and error bars represent the Means ± SEM, respectively. *p < 0.05, **p < 0.01 verse Con, ##p < 0.01 verse HY using repetitive measurement deviation analysis.

have showed that mice sharing the same genetic background exhibited different gut microbiota compositions when raised in different environments, diversifying intestinal mucus properties [26]. Commensal bacteria can prevent pathogenic infection and generate shortchain fatty acid under normal conditions. Short chain fatty acid can serve as the energy source for the colonocytes and are commonly attributed to improvements of the gut barrier by suppressing mucosal nuclear factor, kappa B (NF-κB), activation [27]. Unique metabolites from specific gut microbes can suppress host immune responses. Altered physiological states like nutrient availability, pH, bile acids and immune phenotype favors colonization of pathobionts. Under such condition, commensal bacteria can provide a microenvironment favoring opportunistic infections, and the pathogen can adapt to such environment, resulting in gut dysbiosis [28]. The invasive pathogens could trigger mucosal immune system and aggravate mucosal inflammation, which contribute to intestinal barrier dysfunction. Pre-existing metabolic disease increases risk of opportunistic infections [29]. Previous work has established that the hyperuricemia is accompanied by abnormal gut microbiota. Increased ratio of Firmicutes/Bacteroidetes was found in hyperuricemia mice [20]. Experimental and clinical settings showed that there is a correlative phenotype of an increased ratio of Firmicutes/Bacteroidetes with barrier dysfunction, mucosal inflammation and pathogenesis of chronic diseases [30]. We observed a low abundance of families Bacteroidaceae and genus Bacteroides in HY group. Bacteroides are responsible for providing nutrients and vitamins to both the host and intestinal microbial residents. The low abundance of Bacteroides disruptes microbiota relationships and provides the specific microenvironment for opportunistic infections [31]. The mechanism that allopurinol exerts on intestinal barrier may attribute to chonges of microbial composition. The opportunistic pathogens Streptococcus, Lactococcus and Staphylococcus were suppressed after treatment with allopurinol. We showed that the instigation of hyperuricemia in mice lacking gut microbiota averted the occurrence of intestinal barrier damage, which may be attributed to that the antibiotic treatment prevented the opportunistic infections [32]. These findings further provided evidences supporting the identified gut microbiota as a central orchestrator in hyperuricemia-induced intestinal barrier dysfunction.

Toll-like receptors (TLRs) have been found to associate with several autoimmune disorders, and play a vital role in the interaction between the host immune system and gut microbiota [33]. TLR4 can recognize various damage-associated molecular patterns and trigger NF-κB activation [34,35]. We showed that both allopurinol and antibiotic treatment inhibit TLR4/NF-κB activation, suggesting a potential signaling pathway. However, antibiotic treatment significantly reduced ZO-1 expression. TLRs are microbial-induced proteins that enhance the intestinal epithelial barrier function through recognition of microbial motifs [36–38]. Yuki et al. showed that the activation of TLR2 increases ZO-1 expresssion [39]. We hypothesize that the reduced ZO-1 is potentially caused by abnormal

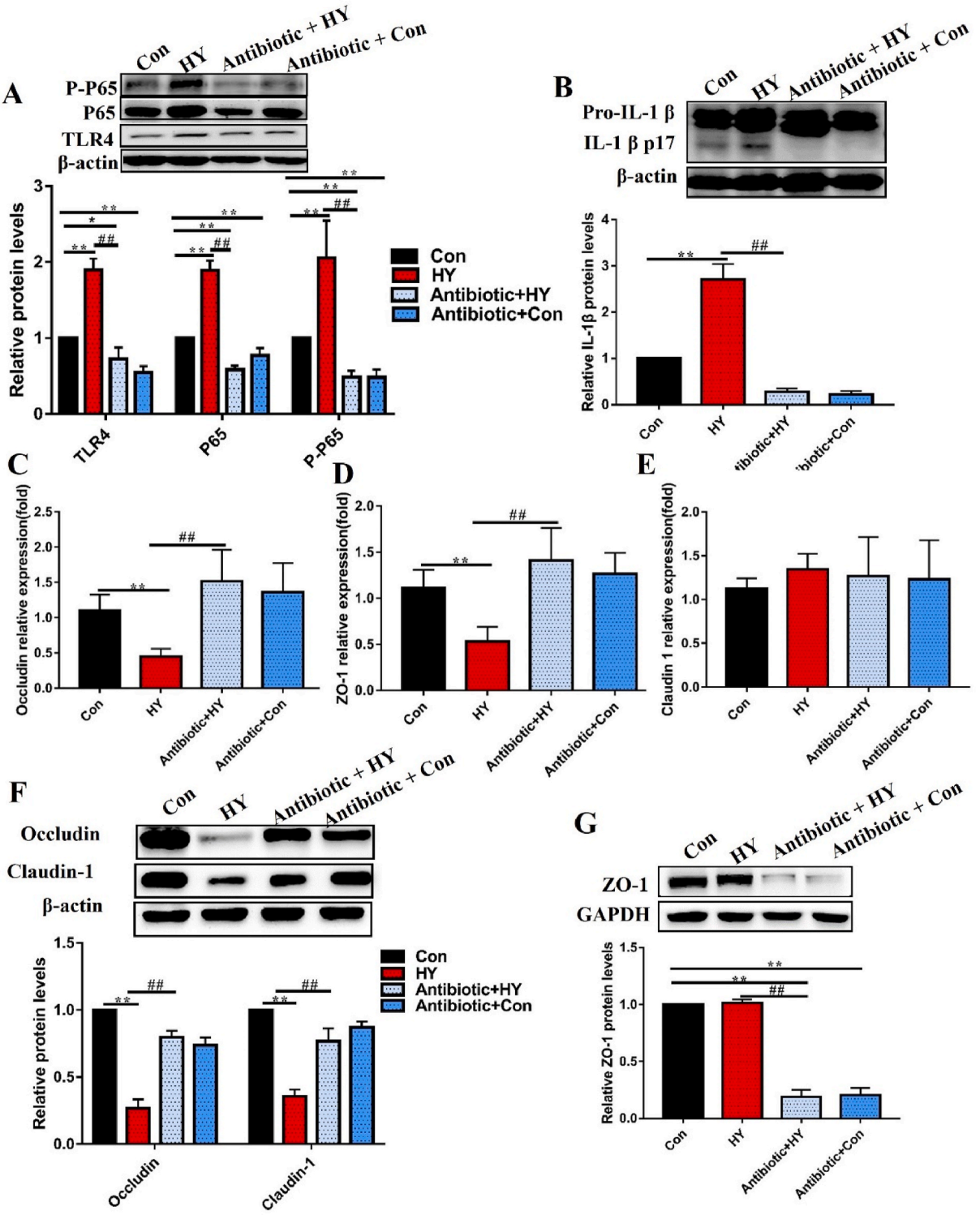

Fig. 7. Gut microbiota regulates intestinal barrier *via* TLR4/P65 signal pathway (A–B) Representative immunoblotting of TLR4, P65 (A) and IL-1β (B) from isolated colon. (C–E) Relative expression levels of Occludin (C), ZO-1 (D) and Claudin1 (E) genes were determined by qPCR from isolated colon. n = 6 mice per group. (F and G) Representative immunoblotting of Occludin, Claudin 1 (F) and ZO-1 (G) from isolated colon. NC, control group; HY, hyperuricemia mice. Bars and error bars represent the Means ± SEM. *p < 0.05, **p < 0.01 verse Con, $^{\#\#}$p < 0.01 verse HY using one-way ANOVA followed by Tukey's multiple comparison post-test.

lower expressions of TLRs due to depletion of microbiota, which may restrain lineage-dependent responses.

Our finidngs highlighted the impact of gut microbiota on intestinal barrier; however, antibiotic treatment did not impede the rise of uric acid. Previous researches have emphasized the crucial role of gut microbiota in hyperuricemia. Liu et al. demonstrated that gut bacteria anaerobically metabolize uric acid. Antibiotic treatments targeting anaerobic bacteria reduce bacterial uric acid genes, potentially elevating the risk of hyperuricemia [40]. Similarly, we also observed a slight increase of uric acid level after antibiotic treatment. However, post-antibiotic treatment did not exacerbate hyperuricemia. Our data showed that pretreatment with antibiotics reduces serum uric acid level. Longitudinal studies suggested that gut dysbiosis precedes and contributes to the development of hyperuricemia [20]. A metagenome analysis on gout patients showed that gut dysbiosis is associated with dysregulated host urate degradation and systemic inflammation [41]. Antibiotic treatment may prevent gut dysbiosis, resulting in lower uric acid level. We utilized adenine and oteracil potassium to establish hyperuricemia model, which was a usual method for building hyperuricemia model. Emerging evidences suggested that the way of these chemicals work can be largely associated with changes in gut microbial diversity and metabolic functions [30]. Similarly, Xie et al. established hyperuricemia mice *via* daily oral gavage of potassium oxonate and hypoxanthine, which was found to company with gut dysbiosis [42]. Thus, treatment with the chemicals in antibiotic-induced microbiota-depleted mice resulted in the reversal of disease severity or less sensitivity to induced disease pathogenesis.

Interestingly, we found that circulating TNF-α in hyperuricemia is not coupled with the restored intestinal barrier. This suggested that additional mechanisms beyond the gut microbiota may contribute to the systemic inflammation. In contrast, allopurinol treatment restored not only intestinal barrier but also effectively normalized systemic inflammation, underscoring the direct effect of uric acid on these processes. Uric acid has been implicated in the activation of inflammatory pathways, leading to the release of pro-inflammatory cytokines and contributing to systemic inflammation [43,44]. Thus, elevated uric acid level may be a key player in systemic inflammation. However, the observed changes in the gut microbial composition following allopurinol treatment further emphasized the bidirectional relationship among hyperuricemia, gut homeostasis and systemic inflammation. Morever, we found that the depletion of gut microbiota aggravates dyslipidemia. Increasing evidences have shown that gut microbiota is indispensable for lipid metabolism [45–47]. Gut microbiota can modify bile acids into secondary bile acids, and the gut microbiota-bile acid crosstalk paly a vital role in lipid metabolism [48–50]. Lynch et al. showed that colonizing mice with bacteria expressing bile-modifying genes from Turicibacter strains decreases serum cholesterol and triglycerides [51]. Consistently, we found also that the bile acid level in hyperuricemia mice is not normal. Noteworthly, lowering uric acid using allopurinol alleviated lipid metabolism, which was accompanied with the alteration in gut microbobial composition.

In our study, we have not identified the specific bacteria that contribute to intestinal barrier and hyperuricemia. What we should do included also to collect the evidences supporting the influence of specific bacteria on intestinal barrier and hyperuricemia. Removing gut microbiota using antibiotic may have attenuated the benefit of gut microbiota. Our further studies should focus on the therapeutic strategies towards modulating gut microbial composition. The application of probiotics, prebiotics, fecal microbiota transplantation among others promises for the management of hyperuricemia and its related complications.

5. Conclusions

Our study carried forward the understanding of hyperuricemia by identifying gut microbiota as a central player in the regulation of intestinal barrier. The complex interplay uncovered has laid a groundwork for future investigations and therapeutic innovations, offered a paradigm shift in the approach to hyperuricemia and its associated metabolic consequences.

Declaration of conflicts of interest

All authors declared no conflict of interest.

Data availability statement

The data associated with the study have been deposited into a publicly available repository. The sequencing data have been deposited at NCBI Sequence Read Archive (https://submit.ncbi.nlm.nih.gov/subs/sra/) with accession numbers (PRJNA1059487).

Ethical declaration statement

All animal experiments were conducted according to established animal welfare guidelines, approved by the Affiliated Hospital of Qingdao University of Animal Care Committee (AHQU-mal2018079). The study complies with all regulations. All procedures were performed in compliance with relevant laws and institutional guidelines, and the appropriate institutional committee has approved them.

CRediT authorship contribution statement

Xiaomin Yang: Writing – review & editing, Writing – original draft, Validation, Methodology, Data curation. **Dan Liu:** Writing – original draft, Validation, Methodology, Data curation. **Xiangzhong Zhao:** Writing – original draft, Visualization, Project administration, Investigation, Funding acquisition, Data curation, Conceptualization. **Yafei Han:** Methodology, Formal analysis, Data curation. **Xiao Zhang:** Validation, Supervision, Methodology, Investigation, Conceptualization. **Quan Zhou:** Validation, Methodology,

Data curation. **Qiulan Lv:** Writing – review & editing, Writing – original draft, Supervision, Methodology, Funding acquisition, Data curation, Conceptualization.

Declaration of competing interest

The authors declare that they have no known competing financial interests or personal relationships that could have appeared to influence the work reported in this paper.

Acknowledgments

This study was funded by National Natural Science Foundation of China (81901575), Shandong Province Natural Science Fund Project (ZR2022MH300).

References

[1] M. Antonella, et al., Serum uric acid concentrations and fructose consumption are independently associated with NASH in children and adolescents, J. Hepatol. 66 (2017).
[2] E.K. Marcus, et al., Uric acid and cardiovascular events: a mendelian randomization study, J. Am. Soc. Nephrol. 26 (2015).
[3] J. Muthukumaran, Q. Shen, Harnessing hyperuricemia to atherosclerosis and understanding its mechanistic dependence, Med. Res. Rev. 41 (2020).
[4] C. Thaiss, et al., Hyperglycemia drives intestinal barrier dysfunction and risk for enteric infection, Science (New York, N.Y.) 359 (2018) 1376–1383.
[5] A. Horowitz, S. Chanez-Paredes, X. Haest, J. Turner, Paracellular permeability and tight junction regulation in gut health and disease, Nat. Rev. Gastroenterol. Hepatol. 20 (2023) 417–432.
[6] J. Martel, et al., Gut barrier disruption and chronic disease, Trends Endocrinol. Metabol.: TEM (Trends Endocrinol. Metab.) 33 (2022) 247–265.
[7] P.D. Cani, et al., Metabolic endotoxemia initiates obesity and insulin resistance, Diabetes 56 (2007) 1761–1772.
[8] M.W. Rohr, C.A. Narasimhulu, T.A. Rudeski-Rohr, S. Parthasarathy, Negative effects of a high-fat diet on intestinal permeability: a review, Advances in nutrition (Bethesda, Md 11 (2020) 77–91.
[9] Y. Cho, B. Song, Pomegranate prevents binge alcohol-induced gut leakiness and hepatic inflammation by suppressing oxidative and nitrative stress, Redox Biol. 18 (2018) 266–278.
[10] Q. Lv, et al., Association of hyperuricemia with immune disorders and intestinal barrier dysfunction, Front. Physiol. 11 (2020) 524236.
[11] Y. Guo, et al., Impaired intestinal barrier function in a mouse model of hyperuricemia, Mol. Med. Rep. 20 (2019) 3292–3300.
[12] Z. Wei, et al., Probiotic Lactiplantibacillus plantarum N-1 could prevent ethylene glycol-induced kidney stones by regulating gut microbiota and enhancing intestinal barrier function, Faseb. J. : official publication of the Federation of American Societies for Experimental Biology 35 (2021) e21937.
[13] H. Atsushi, N. Takeo, F. Takuya, T. Ikumi, Extra-renal elimination of uric acid via intestinal efflux transporter BCRP/ABCG2, PLoS One 7 (2012).
[14] C. Zhao, et al., Gut dysbiosis induces the development of mastitis through a reduction in host anti-inflammatory enzyme activity by endotoxemia, Microbiome 10 (2022) 205.
[15] Q. Ma, et al., Soluble uric acid inhibits β2 integrin-mediated neutrophil recruitment in innate immunity, Blood 139 (2022) 3402–3417.
[16] M.M. Hughes, L.A.J. O'Neill, Metabolic Regulation of NLRP3, vol. 281, 2018, pp. 88–98.
[17] J. Burgueño, M. Abreu, Epithelial Toll-like receptors and their role in gut homeostasis and disease, Nat. Rev. Gastroenterol. Hepatol. 17 (2020) 263–278.
[18] C.T. Capaldo, et al., IFN-γ and TNF-α-induced GBP-1 inhibits epithelial cell proliferation through suppression of β-catenin/TCF signaling, Mucosal Immunol. 5 (2012) 681–690.
[19] Z. Duan, et al., The association between BMI and serum uric acid is partially mediated by gut microbiota, Microbiol. Spectr. 11 (2023) e0114023.
[20] Q. Lv, et al., A dynamics association study of gut barrier and microbiota in hyperuricemia, Front. Microbiol. 14 (2023) 1287468.
[21] D.A. Winer, H. Luck, S. Tsai, S. Winer, The intestinal immune system in obesity and insulin resistance, Cell Metabol. 23 (2016) 413–426.
[22] A. Tripathi, et al., The Gut-Liver axis and the Intersection with the Microbiome, vol. 15, 2018, pp. 397–411.
[23] Björn Meijers, et al., Intestinal Barrier Function in Chronic Kidney Disease, Toxins (Basel) 10 (2018) 298.
[24] T.O. Crişan, et al., Soluble uric acid primes TLR-induced proinflammatory cytokine production by human primary cells via inhibition of IL-1Ra, Ann. Rheum. Dis. 75 (2016) 755–762.
[25] T. Takiishi, C.I.M. Fenero, N.O.S. Câmara, Intestinal barrier and gut microbiota: shaping our immune responses throughout life, Tissue Barriers 5 (2017) e1373208.
[26] H.E. Jakobsson, et al., The composition of the gut microbiota shapes the colon mucus barrier, EMBO Rep. 16 (2015) 164–177.
[27] P. Dey, Targeting gut barrier dysfunction with phytotherapies: effective strategy against chronic diseases, Pharmacol. Res. 161 (2020) 105135.
[28] C. Tropini, How the physical environment shapes the microbiota, mSystems 6 (2021) e0067521.
[29] F. Rossi, C. Amadoro, G. Colavita, LactobacillusMembers of the genus complex (lgc) as opportunistic pathogens: a review, Microorganisms 7 (2019).
[30] P. Dey, The role of gut microbiome in chemical-induced metabolic and toxicological murine disease models, Life Sci. 258 (2020) 118172.
[31] B. Yu, et al., A new polysaccharide from Hawk tea: structural characterization and immunomodulatory activity associated with regulating gut microbiota, Food Chem. 418 (2023) 135917.
[32] R. Wang, et al., Gut microbiota shape the inflammatory response in mice with an epithelial defect, Gut Microb. 13 (2021) 1–18.
[33] D. Talipova, A. Smagulova, D. Poddighe, Toll-like receptors and celiac disease, Int. J. Mol. Sci. 24 (2022).
[34] R.K. Boyapati, A.G. Rossi, J. Satsangi, G.T. Ho, Gut mucosal DAMPs in IBD: from mechanisms to therapeutic implications, Mucosal Immunol. 9 (2016) 567–582.
[35] M. Yamamoto, et al., Cutting edge: a novel Toll/IL-1 receptor domain-containing adapter that preferentially activates the IFN-beta promoter in the Toll-like receptor signaling, J. Immunol. (169) (2002) 6668–6672.
[36] S. Rakoff-Nahoum, J. Paglino, F. Eslami-Varzaneh, S. Edberg, R. Medzhitov, Recognition of commensal microflora by toll-like receptors is required for intestinal homeostasis, Cell 118 (2004) 229–241.
[37] J.F. Burgueño, M.T. Abreu, Epithelial Toll-like Receptors and Their Role in Gut Homeostasis and Disease, vol. 17, 2020, pp. 263–278.
[38] A.E. Price, et al., A map of toll-like receptor expression in the intestinal epithelium reveals distinct spatial, cell type-specific, and temporal patterns, Immunity 49 (2018) 560–575.e566.
[39] T. Yuki, et al., Activation of TLR2 enhances tight junction barrier in epidermal keratinocytes, J. Immunol. (187) (2011) 3230–3237.
[40] Y. Liu, et al., A widely distributed gene cluster compensates for uricase loss in hominids, Cell 186 (2023) 4472–4473.
[41] Y. Chu, et al., Metagenomic analysis revealed the potential role of gut microbiome in gout, NPJ biofilms and microbiomes 7 (2021) 66.
[42] D. Xie, et al., Anti-hyperuricemic, nephroprotective, and gut microbiota regulative effects of separated hydrolysate of α-lactalbumin on potassium oxonate- and hypoxanthine-induced hyperuricemic mice, Mol. Nutr. Food Res. 67 (2023) e2200162.
[43] Q. Ma, R. Immler, Soluble uric acid inhibits β2 integrin-mediated neutrophil recruitment in, Innate Immun. 139 (2022) 3402–3417.
[44] M.M. Hughes, L.A.J. O'Neill, Metabolic regulation of NLRP3, Immunol. Rev. 281 (2018) 88–98.
[45] X. Zhang, P. Gérard, Diet-gut microbiota interactions on cardiovascular disease, Comput. Struct. Biotechnol. J. 20 (2022) 1528–1540.
[46] K. Frazier, et al., Gut microbes and the liver circadian clock partition glucose and lipid metabolism, J. Clin. Invest. 133 (2023).

[47] M. Schoeler, et al., The interplay between dietary fatty acids and gut microbiota influences host metabolism and hepatic steatosis, Nat. Commun. 14 (2023) 5329.
[48] Q. Wang, et al., Gut microbiota regulates postprandial GLP-1 response via ileal bile acid-TGR5 signaling, Gut Microb. 15 (2023) 2274124.
[49] H. Xu, et al., Gut microbiota-bile acid crosstalk regulates murine lipid metabolism via the intestinal FXR-FGF19 axis in diet-induced humanized dyslipidemia, Microbiome 11 (2023) 262.
[50] J. Cai, B. Rimal, C. Jiang, J. Chiang, A. Patterson, Bile acid metabolism and signaling, the microbiota, and metabolic disease, Pharmacol. Therapeut. 237 (2022) 108238.
[51] J. Lynch, et al., Gut microbiota Turicibacter strains differentially modify bile acids and host lipids, Nat. Commun. 14 (2023) 3669.